Science of the Total Environment 912 (2024) 169476

Contents lists available at ScienceDirect

Science of the Total Environment

journal homepage: www.elsevier.com/locate/scitotenv

Global groundwater droughts are more severe than they appear in hydrological models: An investigation through a Bayesian merging of GRACE and GRACE-FO data with a water balance model

Ehsan Forootan [a], Nooshin Mehrnegar [a,*], Maike Schumacher [a], Leire Anne Retegui Schiettekatte [a], Thomas Jagdhuber [b,c], Saeed Farzaneh [d], Albert I.J.M. van Dijk [e], Mohammad Shamsudduha [f], C.K. Shum [g]

[a] Geodesy Group, Department of Sustainability and Planning, Aalborg University, Rendburggade 14, Aalborg 9000, Denmark
[b] Microwaves and Radar Institute, German Aerospace Center, 82234 Wessling, Germany
[c] Institute of Geography, University of Augsburg, 86159 Ausburg, Germany
[d] School of Surveying and Geospatial Engineering, College of Engineering, University of Tehran, Tehran, Iran
[e] Fenner School of Environment & Society, College of Science, Australian National University, Canberra, Australia
[f] Institute for Risk and Disaster Reduction, University College London (UCL), Gower Street, London WC1E 6BT, United Kingdom
[g] Division of Geodetic Science, School of Earth Sciences, Ohio State University, Columbus, OH, USA

HIGHLIGHTS

- An integration of satellite-derived water storage estimates is necessary for improving the estimates of groundwater droughts
- Data-driven ENSO related groundwater droughts are more severe and longer than model estimates
- Global groundwater droughts are underestimated in most of the large-scale river basins worldwide
- The Europe's prolonged droughts of 2017-2021 are better reflected in data sets that are merged with GRACE(-FO) data
- Monitoring groundwater droughts in basins with pronounced multi-year fluctuations (e.g., Danube and Ob) remains challenging

GRAPHICAL ABSTRACT

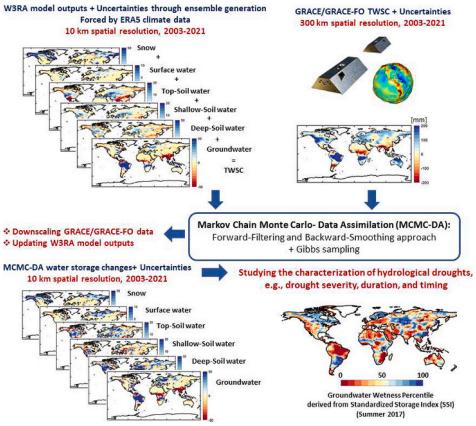

ARTICLE INFO

Editor: Kai Zhang

2000 MSC:
0000
1111

ABSTRACT

Realistic representation of hydrological drought events is increasingly important in world facing decreased freshwater availability. Index-based drought monitoring systems are often adopted to represent the evolution and distribution of hydrological droughts, which mainly rely on hydrological model simulations to compute these indices. Recent studies, however, indicate that model derived water storage estimates might have difficulties in adequately representing reality. Here, a novel Markov Chain Monte Carlo - Data Assimilation (MCMC-

* Corresponding author.
E-mail address: Nooshinm@plan.aau.dk (N. Mehrnegar).

https://doi.org/10.1016/j.scitotenv.2023.169476
Received 9 June 2023; Received in revised form 26 November 2023; Accepted 16 December 2023
Available online 23 December 2023

PACS:
0000
1111
Keywords:
Groundwater droughts
Large scale hydrology
GRACE/GRACE-FO
Drought indices
Bayesian merging
Data assimilation
MCMC merger

DA) approach is implemented to merge global Terrestrial Water Storage (TWS) changes from the Gravity Recovery And Climate Experiment (GRACE) and its Follow On mission (GRACE-FO) with the water storage estimations derived from the W3RA water balance model. The modified MCMC-DA derived summation of deep-rooted soil and groundwater storage estimates is then used to compute 0.5° standardized groundwater drought indices globally to show the impact of GRACE/GRACE-FO DA on a global index-based hydrological drought monitoring system. Our numerical assessment covers the period of 2003–2021, and shows that integrating GRACE/GRACE-FO data modifies the seasonality and inter-annual trends of water storage estimations. Considerable increases in the length and severity of extreme droughts are found in basins that exhibited multi-year water storage fluctuations and those affected by climate teleconnections.

1. Introduction

Drought is a complex phenomenon whose severity periods may cover months and even years (Mishra and Singh, 2010; Van Loon and Laaha, 2015; Van Loon, 2015). It impacts livelihoods and causes disasters such as agricultural losses, water scarcity, and famine (Sheffield and Wood, 2012; Smith and Katz, 2013). Several studies argue that the likelihood of more frequent and stronger droughts will increase due to climate change and other anthropogenic influences (Dai, 2013; Toreti et al., 2022). This necessitates the development of drought monitoring and forecasting systems (Pozzi et al., 2013; Dutra et al., 2014), which are important tools for water resources management and should be further complemented by drought forecasting facilities (Pozzi et al., 2013).

Available drought monitoring methods are often index-based, considering one or more hydro-climatic variables to generate the desired indices summarizing the severity and timing of drought events. Drought indices are calculated by applying statistical approaches to analyze the historical pattern of the hydro-climatic record (see a review of drought monitoring systems in (Hao et al., 2017)). Meteorologically-driven droughts are often characterized using precipitation and precipitation-evapotranspiration records, e.g., the Standardized Precipitation Index (SPI) (McKee et al., 1993; Guttman, 1999) and the Standardized Precipitation-Evapotranspiration Index (SPEI) (Vicente-Serrano et al., 2010). Hydrologically-driven droughts are expressed in storage or moisture contents, e.g., the Standardized Storage Index (SSI) (Mishra and Singh, 2010), which uses soil moisture or groundwater data. Multivariate drought indices are also defined by relating *SPI* or *SPEI* and *SSI*, see e.g., (Hao and AghaKouchak, 2013; Carrão et al., 2016; Forootan et al., 2019). Therefore, a reliable estimation of hydrological drought indices requires more accurate and consistent (e.g., between storage changes and water fluxes) observation records.

Generally speaking, hydro-climatic variables can be measured by in-situ and remote sensing instruments or simulated by models. Though in-situ networks are extremely helpful for understanding water cycle processes, they are limited by spatial and temporal data gaps and instrumental and human errors. Extrapolation of in-situ measurements outside their spatial and temporal observational domain will often introduce considerable uncertainty. Remote sensing techniques provide an alternative opportunity to measure the required variables with bigger spatial coverage compared to in-situ measurements (Yang et al., 2013; Famiglietti et al., 2015; Frappart and Ramillien, 2018). However, these instruments typically measure electromagnetic radiance or returned radar pulses reflected from the Earth's surface. The relationship between these measurements and hydro-climatic variables might be complex and uncertain (Dutta, 2015; Uebbing et al., 2017). Hydrological and climate models provide key variables such as evapotranspiration, soil moisture, and groundwater storage. Nevertheless, inaccurate inputs and forcing fields, data deficiencies (e.g., limited ground-based observations), and imperfect (non-physics based/empirical) modeling assumptions introduce uncertainties into their simulations (Liu and Gupta, 2007).

To address the respective disadvantages, merging existing model outputs with remote sensing observations through Data Assimilation (DA) has gained particular interest, see, e.g., the Global Land Data Assimilation System (https://ldas.gsfc.nasa.gov/gldas) and (Kumar et al., 2022). DA provides important advantages, including (i) the extension of the measurements from a single time and space to be spatially and temporally continuous, (ii) the interpretation of measurements on the basis of physical relationships embedded within the models, (iii) and the weighing of the various uncertainties associated with the model inputs and the measurements (Xu et al., 2014; Schumacher, 2016; Ahmadalipour et al., 2017; Mehrnegar et al., 2020a; Forootan and Mehrnegar, 2022). DA also allows to use directly sensed surface parameters, such as back-scatter or brightness temperature as an input to the models, which are not physical variables in the model, but their relative dynamics might be linked to these parameters (van Dijk et al., 2018; Baguis et al., 2022).

Without DA, global models might be less efficient in simulating hydrological processes and phenomena, such as trends and seasonal and inter-annual variations of water storage, as shown, e.g., by (Mehrnegar et al., 2020a; Scanlon et al., 2018; Mehrnegar et al., 2020b). Therefore, we expect that applying model-derived fields to estimate drought indices, e.g., SSIs, would show limitations in representing the characteristics of hydrological drought events. Therefore, the focus of this study is to quantify the possible contribution of remotely sensed water storage for modifying the relevant estimates of large-scale hydrological models, and subsequently, the characterization of hydrological droughts.

DA of the remotely sensed Surface Soil Moisture (SSM that is referred to as amount of water in a few cm of top soil layers) data has shown promising results in improving the top layer soil water storage changes and in modifying surface energy flux exchanges (Reichle and Koster, 2005; Xu et al., 2015; Lievens et al., 2015; Tangdamrongsub et al., 2020). However, such efforts have less impact on deeper water storage estimates. Therefore, in this study, to modify the storage estimates of all vertical land layers, we assess the impact of integrating Terrestrial Water Storage (TWS) variations derived from the Gravity Recovery And Climate Experiment (GRACE) (Tapley et al., 2004) and its Follow-on mission (GRACE-FO) (Tapley et al., 2019; Landerer et al., 2020) on the computation of storage-based hydrological drought indices. TWS variations represent a vertical integration of water content changes in the surface water, soil moisture, groundwater, and biomass, and can be used to improve the estimation of water states simulated by hydrological models (Mehrnegar et al., 2020a; Zaitchik et al., 2008; van Dijk et al., 2014; Girotto et al., 2016; Khaki et al., 2018; Schumacher et al., 2018; Bolaños Chavarría et al., 2022). Although GRACE/GRACE-FO has previously been used to study hydrological droughts (Forootan et al., 2019; Houborg et al., 2012; Sinha et al., 2017; Zhao et al., 2017) and has been integrated into drought monitoring systems, for example, that of the USA (https://grace.jpl.nasa.gov/applications/drought-monitoring/), its impact on the characteristics of hydrological droughts (including, for example, drought severity, duration, and timing) has not been thoroughly investigated. Adding such investigation is indeed a major focus

of this study.

Applying DA to merge any types of observations with hydrological models does not automatically and always improve simulations. Adding new inputs may also violate the water balance equation that relates water fluxes (precipitation, evapotranspiration and runoff) to water storage changes (Pan and Wood, 2006; Pan et al., 2012). For example, (Girotto et al., 2017) pointed out that assimilating GRACE TWS changes can introduce unrealistic trends in simulated storage compartments or worsen the simulation of evapotranspiration. Conversely, in other cases, DA has no significant impact on the simulation of individual water states or fluxes, as demonstrated in, e.g., (Schumacher et al., 2018).

In this study, we apply a newly established Bayesian DA approach, Markov Chain Monte Carlo-Data Assimilation (MCMC-DA) (Mehrnegar et al., 2020b), to merge GRACE and GRACE-FO TWS changes with the Worldwide Water Resources Assessment (W3RA) (van Dijk, 2010) model and to estimate hydrological variables globally for 2003–2021. MCMC-DA provides the ability to separate GRACE/GRACE-FO TWS changes into its individual compartments (e.g., canopy, snow, surface water, soil water, and groundwater storage) using W3RA model outputs as a priori information of water storage compartments. This technique is comprehensively evaluated against groundwater observations within the USA, see (Mehrnegar et al., 2020b). An evaluation within Bangladesh has been added in the Appendix A. Our motivation to select W3RA as our basis is due to its relatively good global performance when compared with other commonly used global hydrological or land surface models (Mehrnegar et al., 2020a; Bolaños Chavarría et al., 2022).

Here, the SSI (Mishra and Singh, 2010) is estimated using the summations of deep-rooted soil water and groundwater simulations of W3RA, before and after implementing the MCMC-DA (Mehrnegar et al., 2020b). The integration covers the entire period of 2003–2021, where the gaps between the GRACE and GRACE-FO missions are filled by methods published previously (Forootan et al., 2020). Our focus is to show (1) to what extent W3RA-derived deep-soil water and groundwater simulations can gain from GRACE/GRACE-FO measurements through MCMC-DA, (2) how much the updated records in (1) can impact the representation of global SSIs, and finally (3) the characteristics of the 2003–2021 droughts globally and in selected basins. For the remainder of this paper, the term 'groundwater storage' refers to the sum of deep-rooted soil water and groundwater storage, unless stated otherwise. This summation is then used to study drought patterns because it can be considered as deep water resources. Besides, the separation between deep-rooted soil water and groundwater storage is considerably uncertain and is influenced by, among others, topography and geology. By considering the summation we avoid introducing extra uncertainty to our investigations.

Another motivation to focus on the drought patterns, related to the deep water storage changes, is that (i) such investigation represents the impact of climate changes on water resources in deep layers, which are often used for irrigation and are important for the growth of deep rooted vegetation; and (ii) we expect that GRACE and GRACE-FO DA would have their largest contribution in these layers, whereas for studying the droughts of SSM, other DA attempts, e.g., driven by DA of remotely sensed SSM might be more appropriate, see e.g., (Mishra et al., 2017).

2. Data and model

2.1. GRACE and GRACE-FO data

In this study, the latest GRACE and GRACE-FO Level 2 (L2) products of the Center for Space Research (CSR, http://www2.csr.utexas.edu/) are used that cover January 2003–June 2017 (GRACE) and June 2018–December 2021 (GRACE-FO), respectively. To generate monthly TWS changes, first the recommended corrections are applied, including changing the degree-1 coefficients by those from (Swenson et al., 2008) and the degree-2 coefficients by that of (Chen et al., 2007). The latest Glacial Isostatic Adjustment (GIA) model of ICE-6G-D(VM5a) GIA model (Argus et al., 2014; Peltier et al., 2015; Richard Peltier et al., 2018) is applied to account for postglacial deformation anomalies. The DDK3 filter (Kusche et al., 2009) is applied to account for correlated errors.

The filtered potential coefficients are resampled to $0.5^\circ \times 0.5^\circ$ gridded TWS changes fields globally. Uncertainties in the TWS changes fields are computed using a collocation technique, as in (Awange et al., 2016; Ferreira et al., 2016), considering the TWS estimates from the CSR, Jet Propulsion Laboratory (JPL), and GeoForschungsZentrum (GFZ) L2 data, respectively.

To fill the gap between GRACE and GRACE-FO data, we followed the approach in (Forootan et al., 2020) who applied an iterative decomposition approach. This reconstruction approach uses the TWS changes derived from the temporal gravity field products of ESA's Swarm mission (Bezděk et al., 2016) as initial values for the missing fields. Next, Independent Component Analysis (ICA, (Forootan et al., 2012; Forootan and Kusche, 2013)) is applied to update these initial values using the statistics existing in the time series of GRACE, GRACE-FO, and Swarm TWS changes fields. This iterative procedure is initially noisy and inhomogeneous because the signal content and noise of Swarm fields are different from those of GRACE and GRACE-FO data. However, the iteration adjusts the empirical independent components to build a consistent evolution derived from the original GRACE and GRACE-FO time series and those of the updated gap values. The reconstructed data can be downloaded from the Github of the Geodesy research group at Aalborg University: https://github.com/AAUGeodesy/Reconstructed-GRACE-GRACE-FO-TWSC.git.

2.2. W3RA water balance model

The Worldwide Water Resources Assessment (W3RA) (van Dijk, 2010) is a grid-distributed water balance model that simulates landscape water storage in the vegetation and soil systems. Here, the original model code (http://wald.anu.edu.au/challenges/water/w3-and-ozwald-hydrology-models/) was modified to be run globally at daily timestep but with $\sim 0.1^\circ \times 0.1^\circ$. As input climate forcing we used ERA5-Land fields (Muñoz Sabater et al., 2019) of precipitation, surface solar radiation downwards, albedo, and 10-meter wind, as well as minimum and maximum temperature (Hersbach and Dee, 2016).

The monthly averaged model states (snow, surface water storage, surface soil water (top layer), shallow-rooted soil water, deep-rooted soil water storage, and groundwater storage), that together comprise the W3RA water storage components were used as a priori information to separate reconstructed TWS changes to its compartments. Model uncertainty is estimated following (Renzullo et al., 2014) by perturbing the forcing data. For this, an additive error is assumed for the short-wave radiation perturbation of 50 Wm^2, a Gaussian multiplicative error of 30% for rainfall perturbation, and a Gaussian additive error of 2 °C for temperature fields. The estimated model uncertainty is used in MCMC-DA as the initial value of the variance/covariance matrix of the unknown state parameters.

2.3. Global river basins

The world's 33 largest river basins are considered to study the SSI evolution. The selected basins are the same as in several previous studies, e.g., (Llovel et al., 2011; Forootan et al., 2014), and the river basin contours are based on masks of 0.5° resolution from (Oki and Sud, 1998). The basins are shown in the Appendix B. From these, we selected the Amazon, Amur, Euphrates, Aral, Caspian, Ob, Yukon, Zambezi, Brahmaputra, Danube, and Mekong River Basins to compute and analyze basin averages from GRACE/GRACE-FO and other products in greater detail. To account for differences in spatial resolution, the

leakage reduction and averaging approach in (Vishwakarma et al., 2017) is implemented in the spectral domain. This approach simultaneously minimizes the summation of leakage-in and leakage-out contributions.

2.4. ENSO index

The El Niño Southern Oscillation (ENSO) is a large-scale ocean–atmosphere interaction in the Tropical Pacific, which affects the climate of many regions of the Earth (Trenberth and Hoar, 1996; Forootan et al., 2016). El Niño refers to the warm phase of ENSO, while its opposite (cold) phase is known as La Niña. The evolution of ENSO is measured by indices, where the Multivariate ENSO Index (MEI, http://www.esrl.noaa.gov/psd/enso/mei/) is the first principal component of the combined fields of sea level pressure, zonal and meridional components of wind, surface air pressure, and total cloudiness fraction. The unit of MEI is normalized here, i.e., the temporal mean is removed, and anomalies are divided by the standard deviations to be compared with the PCA investigation of changes in water storage and drought indices. For example, Anyah et al. (2018) compared MEI with the Niño 3.4 indices and found negligible differences between their correlation values.

The time-variable Terrestrial Water Storage $TWS(t)$, with t representing time, reflects difference between precipitation $P(t)$ as mass input minus evapo-transpiration $E(t)$, runoff $R(t)$, and the water storage at the previous time step $t-1$, at any given location. This can be written as the water balance equation: $TWS(t) = TWS(t-1) + P(t) - E(t) - R(t)$, where the units are in Equivalent Water Height (EWH). ENSO directly impacts the temperature and precipitation, globally. This and changes in the available water in land lead to changes in the distribution of evapotranspiration and river discharge, see, e.g., (Phillips et al., 2012; Scanlon et al., 2022). As a result, the integral effect of ENSO can be reflected in GRACE and GRACE-FO TWS changes because they are related to changes in water fluxes through the water balance equation (Anyah et al., 2018; Eicker et al., 2016). The ENSO's impact on fluxes might be detected faster than its effects on TWS changes because of the memory of hydrological processes and the processes driving the exchanges between various water storage and water flux states that can add delays to this evolution. Besides, in this study, we evaluate changes of the deep soil water storage and groundwater storage. Therefore, it is expected that the vertical and lateral under-surface hydrological exchanges cause differences in the phase and magnitude of ENSO impact on evolution of these deep water resources. To account for such 'out-of-phase' variability, we apply the Hilbert transformation on the normalized MEI. Therefore, the original MEI and the transformed one would represent all (semi-)cyclic components that are associated with the instantaneous ENSO and its out-of-phase effects, see also (Phillips et al., 2012).

3. Methods

3.1. MCMC-DA for merging GRACE/GRACE-FO data with models

MCMC-DA is a Bayesian approach to merge GRACE-like TWSC data with models, which was introduced in (Mehrnegar et al., 2020b). This approach takes advantage of the multi-variate 'state-space model' (Bernstein, 2005) (Eqs. (1) and (2)), which is used to recursively update individual water storage components from the W3RA (as a priori information), and taking GRACE/GRACE-FO TWS changes as observations. This is written as:

$$Y_t = Z_t\Theta_t + \varepsilon_t, \tag{1}$$

$$\Theta_t = \Theta_{t-1} + \delta_t. \tag{2}$$

where Eqs. (1) and (2) are the 'observation equation' and the 'state equation' of the multivariate state-space model, respectively. This means that a linear relationship is assumed between GRACE/GRACE-FO TWS variations (Y_t) and the modeled individual water storage components from W3RA (Z_t) using the unknown state parameters Θ_t. In these equations, ε_t and δ_t are the residuals that are assumed to be Gaussian distributed and independent from each other with a mean value of zero and an error covariance matrix of V_t and Q, respectively. These formulations allow both state parameters and error covariance matrix of the additive innovations to vary in time, where $t = 1, 2, \ldots, T$ is the time step, and T the length of the time series (223 months). Uncertainty in GRACE/GRACE-FO TWS changes is reflected in V_t, while the error covariance matrix Q corresponds to the error vector δ_t, and defines the unknown temporal dependency between water storage changes at each time point to previous time steps.

Within the procedure of MCMC-DA, the unknown state parameters (δ_t) and temporal dependency between them (Q) are estimated using Gibbs sampling (Gelfand and Smith, 1990; Smith and Roberts, 1993), where the joint posterior distribution of the unknown parameters is estimated using the forward-filtering backward-smoothing recursion approach as in (Kitagawa, 1987). Full details and equations of this MCMC-DA approach can be found in (Mehrnegar et al., 2020b).

Here, we apply the MCMC-DA to merge T = 223 months (between 2003 and 2021) of reconstructed GRACE/GRACE-FO TWS data with those of W3RA. The estimated storage of the top-soil, shallow-rooted soil, and groundwater compartments can be found from: https://github.com/AAUGeodesy/MCMC-DA-water-storage-changes.git. An example of the water storage separation using the original W3RA model and MCMC-DA within the Euphrates River Basin is provided in Appendix C.

3.2. Standardized Storage Index (SSI)

SSI can be interpreted as a hydrological drought index, which is computed here based on the probabilistic behavior of water storage changes time series. To compute SSI, we first removed the linear trend of 1980–2021 derived from the global run of the W3RA model. This trend reduction assumes that the bias between model outputs and GRACE/GRACE-FO measurements is temporally invariant, see an example in (Forootan et al., 2019). The remaining linear trend of 2003–2021 is considered to be a result of the climate change and anthropocentric impacts, whose signals are of interest of this study. To concentrate on the GRACE and GRACE-FO era, we then fit a gamma probability density function to the water storage changes of 2003–2021 and compute their cumulative distribution. These are then transformed to standard normal distributions following (Wu et al., 2001). The transformed probability varies between 3.0 and −3.0 (Edwards, 1997), which can be interpreted as drought unit or the level of wetness and dryness, respectively.

3.3. Principal component analysis (PCA)

PCA (Jolliffe, 1986) is applied in this study to explore spatial and temporal data records, through the Singular Vector Decomposition (SVD) that expands data sets (such as $\mathbf{X}$) in terms of new sets of empirical base functions, i.e.,

$$\mathbf{X} = \widetilde{\mathbf{P}}_k\Lambda_k\widetilde{\mathbf{E}}_k^{\mathrm{T}} = \widetilde{\mathbf{P}}_k\mathbf{E}_k^{\mathrm{T}} = \mathbf{P}_k\widetilde{\mathbf{E}}_k^{\mathrm{T}}. \tag{3}$$

The matrix $\mathbf{E} = \Lambda\widetilde{\mathbf{E}}$ contains spatial Empirical Orthogonal Functions (EOFs). The EOFs in $\mathbf{E}$ represent anomaly maps that carry the unit of data sets and $\widetilde{\mathbf{E}}$ contains unit-less eigenvectors, see, e.g., (Forootan et al., 2012). Entries of $\mathbf{E}$ or $\widetilde{\mathbf{E}}$ are associated with the unit-less matrix $\widetilde{\mathbf{P}}$ or $\mathbf{P}$, respectively, whose columns are temporally uncorrelated and known as Principal Components (PCs). In Eq. (3), k is the number of retained

modes that represent the dominant portion of variance to reconstruct the original data matrix **X**. The portion of the variance of each mode (e.g., V_k) can be computed by dividing the quadratic values of the corresponding singular value by the sum of the squares of all singular values, i.e.,

$$V_k = \Lambda_k^2 \Big/ \sum(\Lambda^2) \tag{4}$$

To compare various global data sets of this study, we made use of the orthogonal and unit-less properties of the EOFs. For example, to compare two data sets **X** and **Y**, PCA (Eq. (3)) is applied on the first data set to decompose it as $\mathbf{X} = \mathbf{P}_\mathbf{X}\widetilde{\mathbf{E}}_\mathbf{X}^T$. Then, the second data set **Y** is projected onto the EOFs of the first data set ($\widetilde{\mathbf{E}}_\mathbf{X}$) as

$$\widehat{\mathbf{P}}_\mathbf{Y} = \mathbf{Y}\widetilde{\mathbf{E}}_\mathbf{X}, \tag{5}$$

where $\widehat{\mathbf{P}}_\mathbf{Y}$ represents the projections of the second data, and can be compared with $\mathbf{P}_\mathbf{X}$.

It is worth mentioning here that the PCA modes, extracted from various data sets of this study, should be considered as statistical modes that reflect a dominant portion of the variance. However, they do not necessarily represent physical processes. Despite this, in the Results section, we will show that some of these modes contain strong correlations with physical processes such as that of ENSO's footprint. Applying more sophisticated data exploration techniques such as complex independent component analysis or non-linear techniques (Eicker et al., 2016; Forootan et al., 2018; Boljka et al., 2022) can be tested to explore their potentials for improving the results.

4. Results

4.1. A global assessment of SSI estimates

Changes in the magnitude and phase of seasonal water storage components could have an impact on the estimation of droughts, especially on their duration and severity. To understand to what extent GRACE/GRACE-FO data might alter the estimation of groundwater storage, the PCA (Eq. (3)) is applied on the corresponding MCMC-DA estimates. The first five PCA modes that are associated with considerably bigger (than the rest of) eigenvalues are selected to be interpreted in this study. For comparison, we also used the computed EOFs as the basis, and the time series of the original W3RA and the SSI from the MCMC-DA and original W3RA are projected onto these EOFs (using Eq. (5)).

Fig. 1 summarizes the results of the first three PCA modes representing 35 %, 17 %, and 9 % of the total variance of groundwater changes, respectively. The first two modes (EOF1 & PC1 and EOF2 & PC2) indicate seasonal changes, with differences in the magnitude of seasonality found to be in the range of (20–120 mm). The differences between the projects of SSI indices (orange and gray colors) indicate that the seasonal differences of the storage estimates are translated to an under- or overestimation of drought severity (i.e., between 0.2 and 0.5 drought unit). The third PCA mode (EOF3 & PC3) of Fig. 1 represents a superposition of semi- and inter-annual differences in the storage changes, which have led to multi-year differences in the SSI estimates. The differences become more evident after the year 2017, where the indices from MCMC-DA indicate that the prolonged global droughts of 2017–2021 are more pronounced than those from the original model.

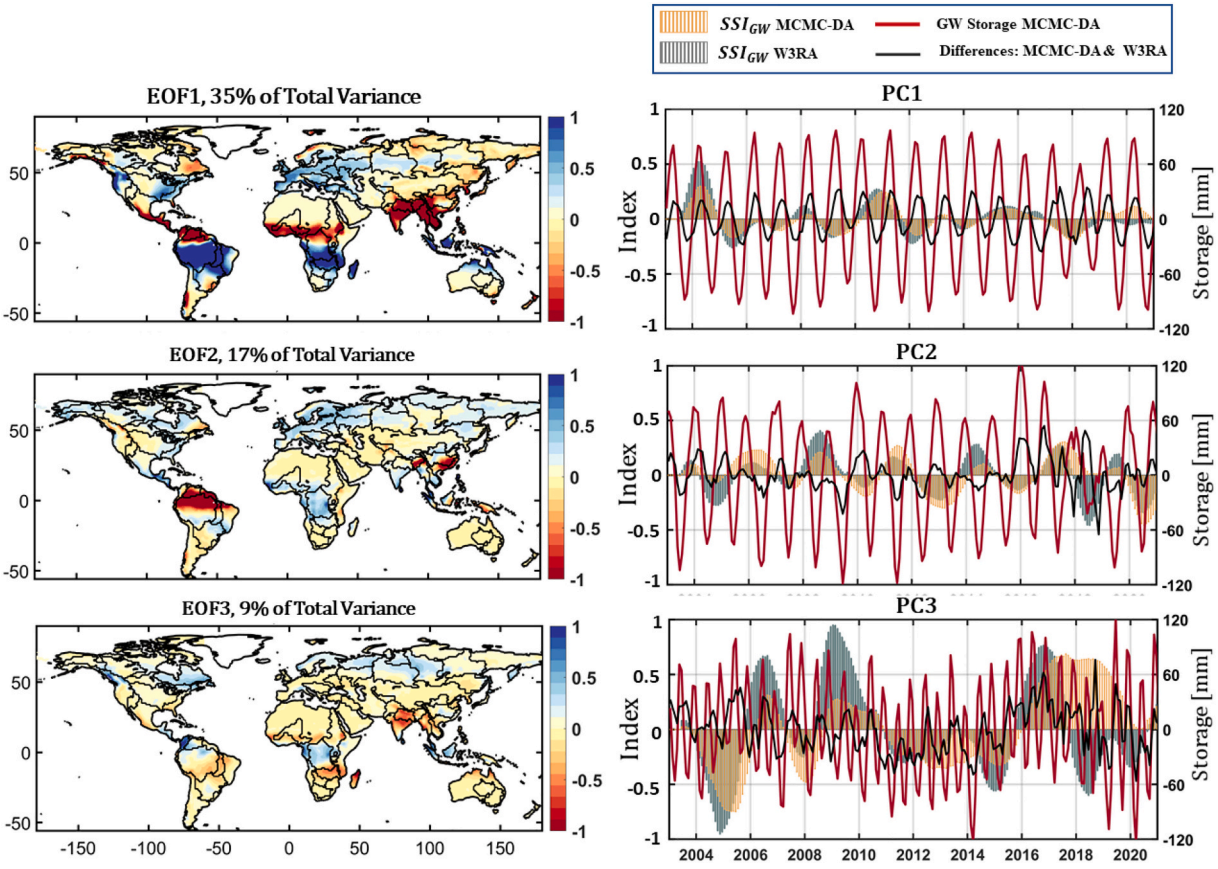

Fig. 1. First 3 modes (EOF & PC) derived from applying PCA on groundwater storage changes (named as "GW storage" in the figure) of MCMC-DA and W3RA, and their associated SSIs (named as "SSI_{GW}").

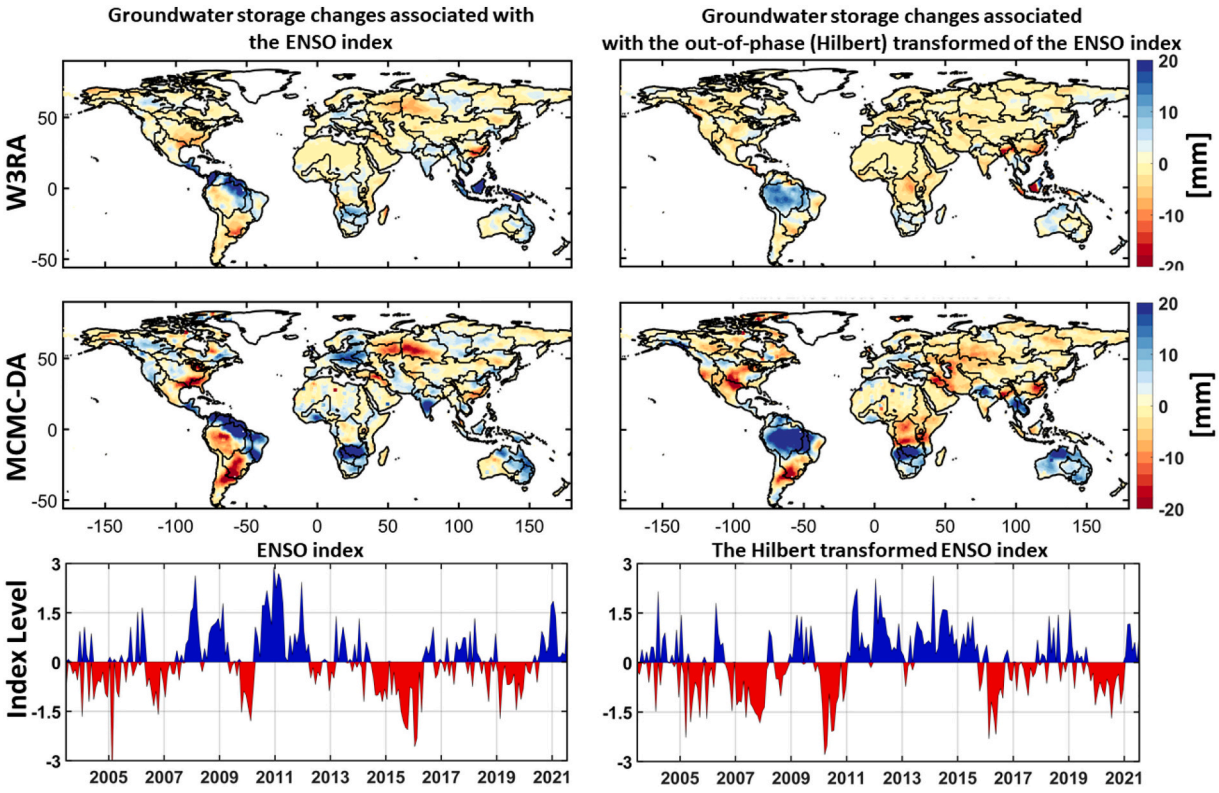

Fig. 2. Groundwater storage changes that are associated with the ENSO index (i.e., the original index and its Hilbert transformed time series). The results are derived from W3RA and MCMC-DA groundwater storage changes, and by fitting a multi-linear regression models described in the text. The top-left and middle-left plots are associated with the ENSO index (bottom-left), those on the right with the Hilbert-transformed (out-of-phase) storage changes.

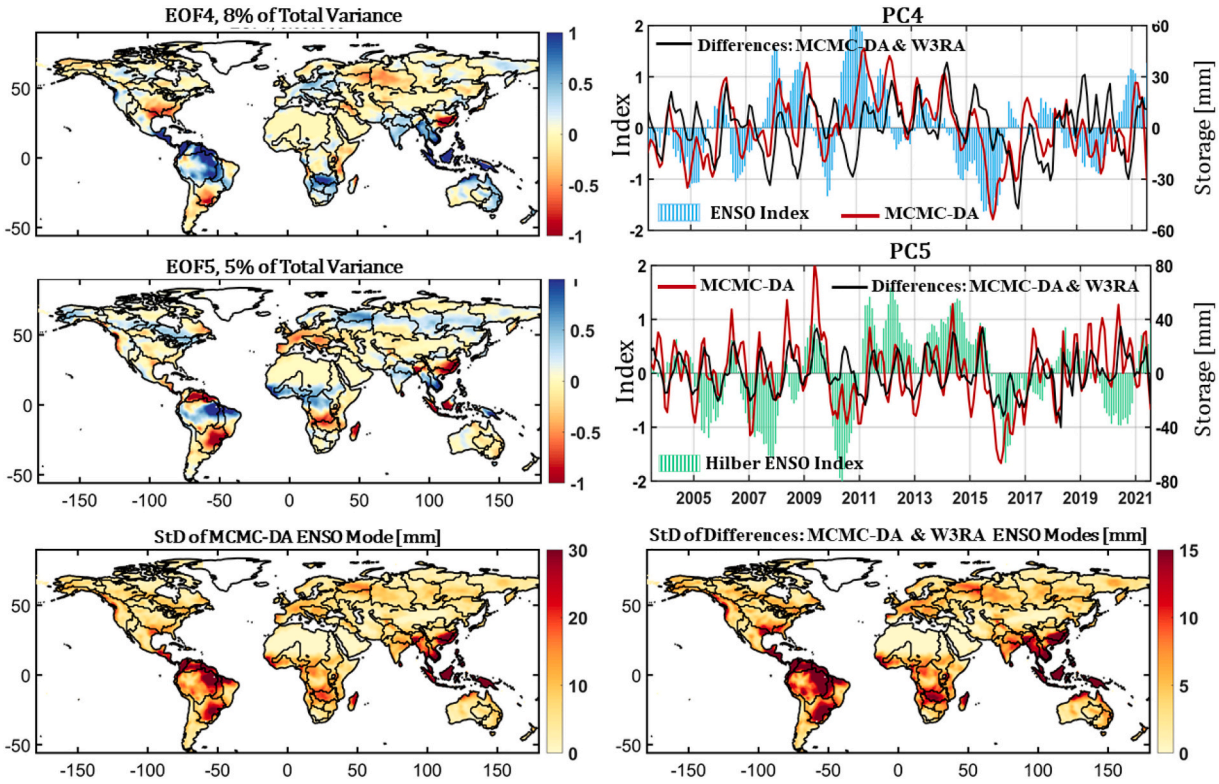

Fig. 3. Mode four (EOF4 & PC4 top-left and -right) and mode five (EOF5 & PC5 middle-left and -right) derived from applying PCA to groundwater storage changes of MCMC-DA and W3RA model outputs. The Standard Deviations (StD) of the ENSO mode ($\widetilde{\mathbf{P}}_{4,5} \times \mathbf{E}^{\mathbf{T}}_{4,5}$) derived from the MCMC-DA groundwater and its difference with original W3RA are shown on bottom-left and -right plots, respectively.

Previous studies (e.g., Anyah et al., 2018; Eicker et al., 2016) have already shown that GRACE TWS variations contain the footprint of teleconnection processes, especially those related to ENSO. To demonstrate how GRACE/GRACE-FO TWS variations might alter the inter- and intra-annual components of water storage changes, we compare the dominant ENSO modes of groundwater storage changes of MCMC-DA with those of W3RA in Fig. 2.

Therefore, we applied a multi-linear regression to extract global water storage changes related to ENSO. For this, a constant term, a linear trend, the seasonal, and ENSO components (with the normalized ENSO index (E) and its Hilbert transform ($H(E)$), $H(.)$ being a Hilbert transformation operator) are fitted to the time series of groundwater storage changes. The last two indices are used to capture the in-phase and out-of-phase patterns of water storage changes due to the ENSO, respectively, see also (Phillips et al., 2012). The global storage time series are stored in the data matrix $\mathbf{X}(\phi,\lambda,t)$. The regression of each gridded time series (associated with the latitude ϕ and longitude λ) will follow $x(\phi,\lambda,t) = a + b\,t + c\cos(2\pi t) + d\sin(2\pi t) + e\cos(4\pi t) + f\sin(4\pi t) + g\,E + h\,H(E(t)) + n(t)$, where $n(t)$ represents temporal random noise and t is time in year. The coefficients a to h carry the same unit as the data sets and can be computed using the least squares approach (Koch, 2007).

The values of a from the original model and MCMC-DA estimates cannot be interpreted because they are referred to the long-term biases, and it is not observed by GRACE and GRACE-FO estimated. Though the coefficients of b to f are considerable, and they are related to the annual and semi-annual components and important, we do not interpret them here because such variations are well discussed in previous hydrological studies, e.g., (Scanlon et al., 2018). The globally distributed coefficients g and h (in mm water storage) are associated with the ENSO and its out-of-phase evolution shown in Fig. 2, where the top plots are from the original W3RA, the middle ones from MCMC-DA and the bottom plots represent the normalized ENSO index and its Hilbert transformed time series. Comparing the plots, it is evident that integrating GRACE/GRACE-FO data increases the magnitude of the ENSO mode (i.e., the ENSO mode of the MCMC-DA is more pronounced, by between 10 and 15 mm for the Amazon River Basin, North Asia, South Africa, and Australia). The influence of ENSO on precipitation changes of these regions is reported in previous studies, see e.g., (Forootan et al., 2016; Davey et al., 2014).

To understand how the differences in the ENSO mode might affect the representation of drought events, we used mode four (EOF4 & PC4) and mode five (EOF5 & PC5) derived from applying PCA as a dominant portion of the global ENSO impact on the evolution of global groundwater storage changes. The spatial and temporal differences between those of MCMC-DA and W3RA are shown in Fig. 3. It is worth mentioning here that ENSO mostly affects the interannual variability of water fluxes and water storage, see, e.g., (Phillips et al., 2012; Eicker et al., 2016; Forootan et al., 2018). Since the trend, as well as annual, and semi-annual components of TWS changes were not removed before applying the PCA in Fig. 3, the ENSO modes appeared on the third and fourth components (i.e., EOF3, 4, PC3, and PC4). If these components had been removed, we expected to extract the dominant part of ENSO in the first two modes, see, e.g., (Forootan et al., 2018). However, a comparison of these modes with the multi-linear analysis of Fig. 2 indicates similarities in the amplitude (i.e., varying between −40 to 40 mm EWH in majority of the global grid), and the pattern of ENSO, which shows that the performance of PCA in extracting the average impact is reasonable.

The differences between the PCs are found to be as big as each individual PC. This is due to the fact that the GRACE/GRACE-FO DA modifies the timing (phase differences) of water storage estimates, as shown in Appendix D, (Fig. D.1). After merging W3RA with GRACE/GRACE-FO TWS changes, temporal correlation coefficients between ENSO index and the ENSO mode of groundwater storage are increased from 0.38 to 0.49, and correlation coefficients between the Hilbert-ENSO index the Hilbert ENSO mode of groundwater storage are increased from 0.29 to 0.36. The standard deviation of the ENSO mode of MCMC-DA groundwater storage is found to be in the range of $5-30$ mm, while the standard deviations of the differences between MCMC-DA and W3RA ENSO modes are found to be in the range of $5-15$ mm (Fig. 3, bottom).

The PCs of the original model output and MCMC-DA were used to compute SSIs, as a measure of global impact on drought representation due to the ENSO. The differences between indices indicate an average 6 months in the timing and 18 months in the duration of the major ENSO-related droughts. Fig. 4 indicates the translation of PC4 and PC5 to SSI. One could expect this impact to be more dominated in ENSO hot spots, where the anomalies of EOF4 and EOF5 (in Fig. 3) are stronger, e.g., in South America, East and South Africa, Australia, the west of North America and, to a less extent, Europe and Asia.

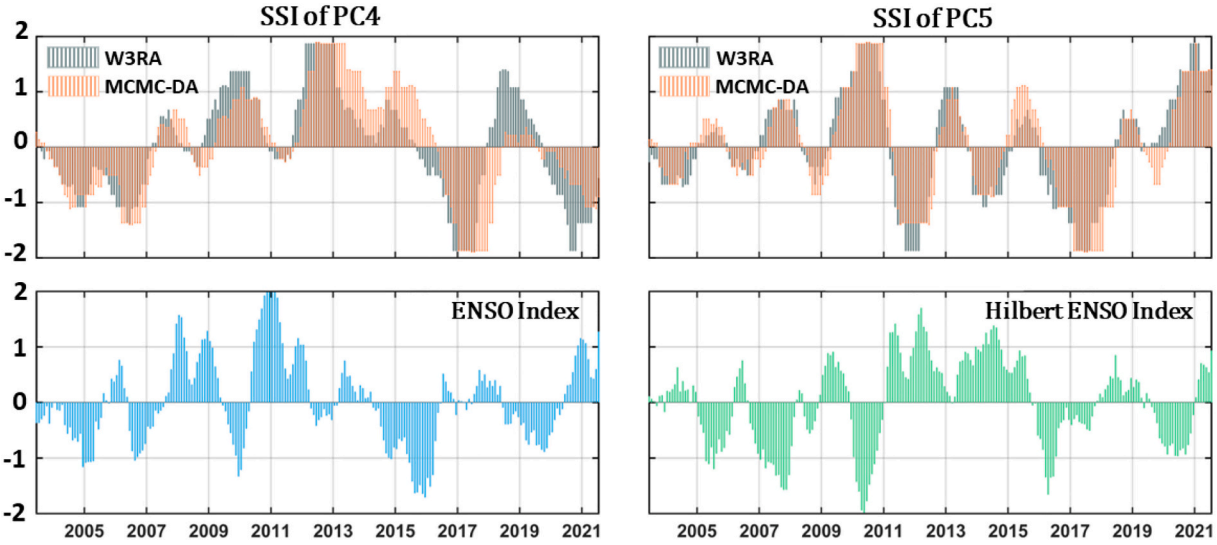

Fig. 4. SSIs translated from PC4 and PC5 of MCMC-DA and W3RA groundwater storage changes in Fig. 3.

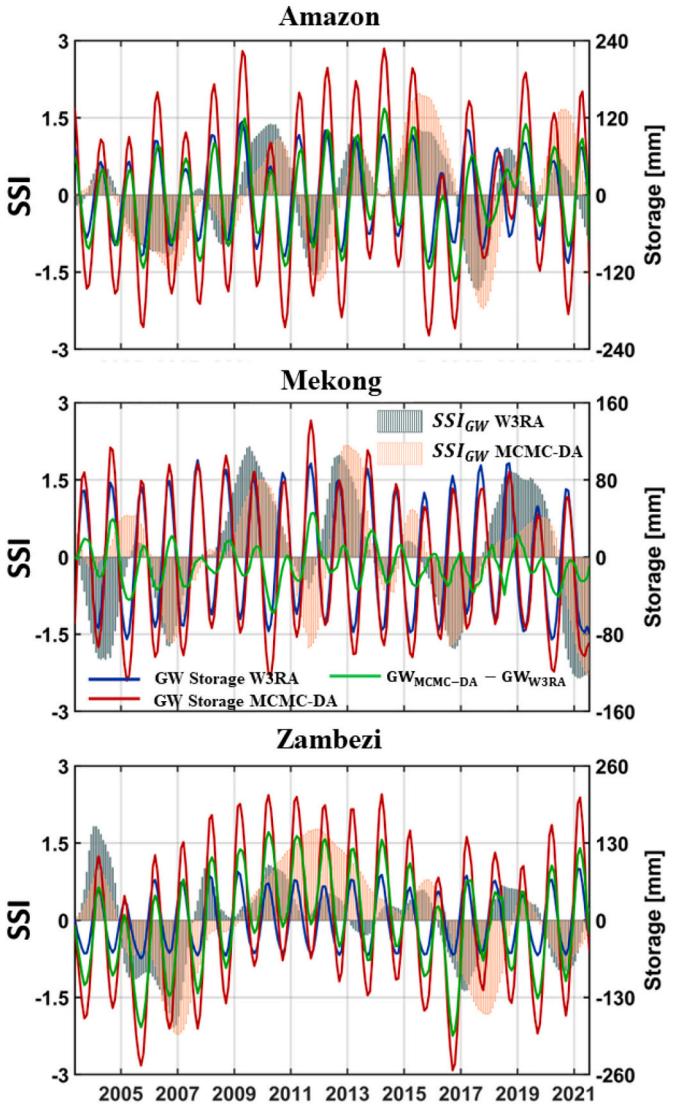

Fig. 5. Basin averaged time series of SSIs and groundwater storage changes derived from W3RA and MCMC-DA within the Amazon (top), Mekong (middle), and Zambezi (bottom) River Basins.

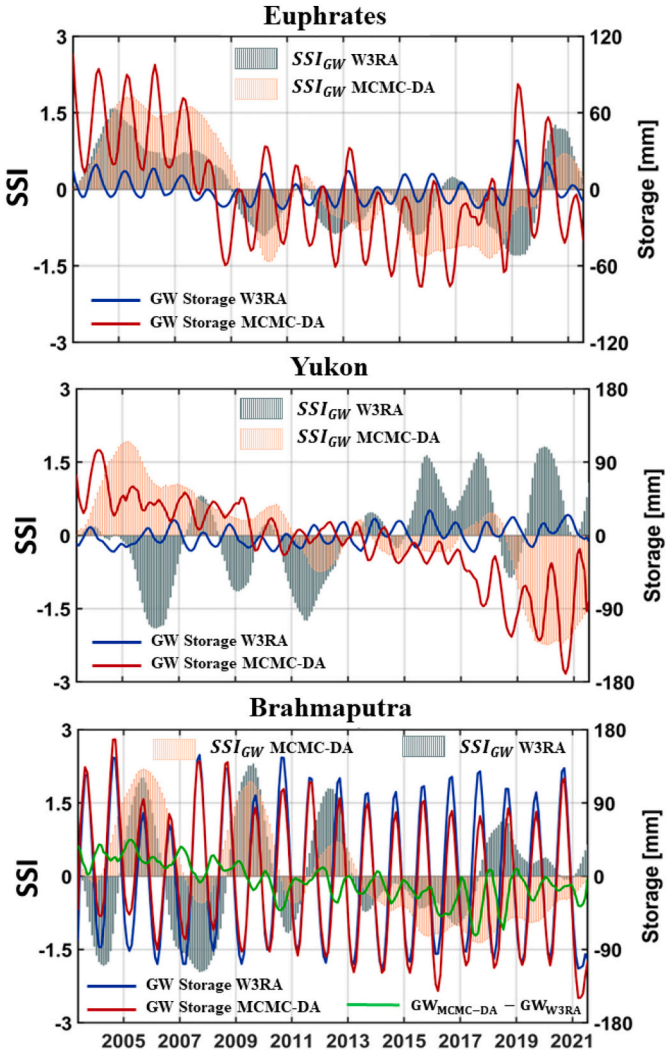

Fig. 6. Basin averaged time series of SSIs and groundwater storage changes derived from W3RA and MCMC-DA within the Euphrates (top), Yukon (middle), and Brahmaputra (bottom) River Basins.

4.2. Characteristics of SSIs in selected large river basins

SSIs are computed from the original W3RA and MCMC-DA derived groundwater storage estimates for the world's 33 largest river basins as defined in (Oki and Sud, 1998, see also Fig. B.1). The results can be found from https://github.com/AAUGeodesy/Standardize-Storage-Indeces.git. Here, we focus on selected basins that experienced different temporal water storage updates after introducing GRACE and GRACE-FO measurements through the MCMC-DA.

4.2.1. Amazon, Mekong, and Zambezi River Basins

In Fig. 5, results for the Amazon (South America), Mekong (Southeast Asia), and Zambezi (South Africa) River Basins are shown, where the storage differences are found to be dominated by the annual component. The amplitude of storage differences in these basins was ~ 80, ~ 15, and ~ 120 mm on average, respectively. Though the storage differences are considerable, we did not find major differences in the magnitude of SSIs in Amazon and Mekong between the original and MCMC-DA outputs, except those of wet periods of 2015–2016, and 2020–2021 in the Amazon, where the latter was found to be more intense (SSI of >2 for MCMC-DA). The main impact of the annual storage differences in these basins is on the timing of the drought periods, especially for the peaks after 2015 in the Amazon and that of 2011 in the Mekong Basin. For example, the wet event of 2020–2021 in the Amazon was found to be six months longer than the SSI of the original model. The water storage time series of Zambezi contained a superposition of the annual and a slow-evolving periodic component with a period of $\sim 10 - 15$ years. This slow process has an impact on the length and magnitude of the extreme events, for example that of 2009–2014 in the Zambezi Basin was more intense (1 unit higher) than the SSI of MCMC-DA (see Fig. 5).

4.2.2. Euphrates, Yukon, and Brahmaputra River Basins

Integrating observed TWS changes into models can introduce distinguished multi-year trends into storage estimates. Depending on the hydrological setting and the history of water storage changes in the

basins, the resulting impact on representing the drought evolution can vary. Here, we focus on the Euphrates (in the Middle East), Yukon (West America), and Brahmaputra (South Asia), where there basins exhibited a long-term water storage decline (Fig. 6).

The Euphrates Basin has been hit by climate change; with less snowfall in winter and hot summers over the last decade (Abdelmohsen et al., 2022) along with heavy extraction for irrigation (see, e.g., Voss et al., 2013; Forootan et al., 2017). The storage depletion in the Euphrates Basin translated to more intensified and prolonged drought events after 2009. The SSIs of the MCMC-DA outputs are found to be around half to one unit drier than those of the original model. We also found that even very wet years (e.g., 2020) did not return the index to strongly positive values.

In the Yukon Basin, a substantial contribution of mountain glaciers on observed TWS variability can be expected, but rather poorly represented in all hydrological models (see, e.g., Zhang et al., 2016). A long-term trend of TWS changes can be detected from MCMC-DA results, which does not appear in the original model estimates. We found a rate of $-5.79\ km^3/year$ TWS changes lost in this basin, consistent with the recent study by (Ferreira et al., 2023). In Yukon, the long-term trend is strongly reflected in the SSI of MCMC-DA, where the occurrence of wet and dry periods is found to be opposite. As the separation of the glacier melt and sub-surface water storage is extremely difficult in this basin (Zhang et al., 2016; Melkonian et al., 2014), the results must be interpreted with caution.

In the Brahmaputra Basin, after integrating the GRACE/GRACE-FO data, the amplitude of the annual peaks decreased. In combination with the overall negative trend this affected the amplitude of SSI estimates. The SSI of MCMC-DA indicated a prolonged drought after 2010, which was not fully recovered after the wet season of 2018. However, the original model suggested that the hydrological drought terminated in 2018, which contrasts with local experience (Parajuli et al., 2021). The time series of differences in Brahmaputra contains a long-term trend ~ -2 mm/year that is likely related to groundwater withdrawal in this basin (Pandey et al., 2020).

4.2.3. Danube and Ob River Basins

The existence of multi-year trends alongside multi-year and seasonal fluctuations in the historical trends represents a considerable impact on the characteristic of SSIs. This can be clearly detected in the Danube River Basin (Europe), where the positive peaks of 2007 and 2012 are considerably underestimated. The impact during major droughts is found to be considerably larger, for example, the severe drought of 2019–2021 (Barbosa et al., 2021) was underestimated by the original model by ~ 2 units. We also found up to 3–6 months differences in the timing of drought development and termination (compare 2013–2014 in Fig. 7).

In the Ob River Basin, MCMC-DA indicates stronger water storage fluctuations. In some years, e.g., 2012, and 2016 their amplitude is relatively stronger (~ 35 and ~ 15 mm, respectively), and coincides with changes in the trend in the water storage time series. As a result, there are clear timing differences in the termination of droughts in 2013–2014 and the extension of the slightly wet episode in 2018–2019, Fig. 7.

5. Conclusions

Large-scale drought events, which strongly influence global and regional water resources, can be determined using water storage estimates, which are often derived from hydrological models. The quality of representing droughts will be to a large extent depends on the quality of model estimates. Here, we applied a novel Bayesian Data Assimilation

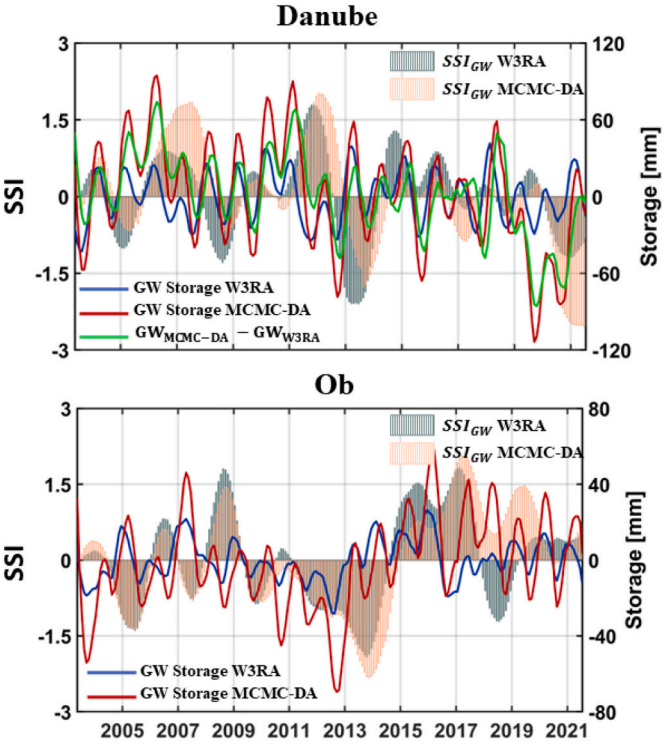

Fig. 7. Basin averaged time series of SSI and groundwater storage derived from W3RA and MCMC-DA within the Danube (top) and Ob (bottom) River Basins.

(MCMC-DA, Mehrnegar et al., 2020b) to merge a gap-filled time series of TWS changes from GRACE and GRACE-FO data with the W3RA global water balance model. The improved estimates of groundwater (i.e., the sum of model deep-rooted soil and groundwater storage) were used to assess to what extent such an integration is important for representing water storage related (i.e., hydrological) drought events. This is done by computing Standardized Storage Indices (SSIs) using the output of the original W3RA model and those of MCMC-DA as input. This study covers the large-scale groundwater changes of 2003–2021 globally, as well as individual large river basins. In summary, we conclude that:

- The PCA of global groundwater storage variations and the corresponding SSIs indicate that seasonal and multi-year differences between the storage estimates of the original model and MCMC-DA can affect the estimates of SSIs. This relationship is not directly proportional, and can translate differently into SSIs depending on the water storage record and the timescale of the differences. Overall, we found that after introducing GRACE and GRACE-FO data, the prolonged drought events of 2016–2021 became more pronounced in South America (e.g., Amazon River Basin), South Africa (e.g., Zambezi River Basin), West America (e.g., Yukon River Basin), and South Asia (e.g., Brahmaputra River Basin). The timing of drought events was also modified on average by ~ 3 months at the time scale of ~ 1.5 years. The results are found to be considerable for drought monitoring applications.
- We found that the integration of GRACE and GRACE-FO data increases the footprint of ENSO in the groundwater storage estimates (up to 40 mm in, e.g., South America, Europe, and South Africa). The translation of ENSO-related water storage estimates into SSI

indicates that ENSO can move the timing of the drought events by 18 months and might change its magnitude by up to 0.8 SSI units.

- In most of the large river basins studied here, we observe an increase in the magnitude, extent, and length of groundwater droughts. In Amazon and Mekong, where the differences between the MCMC-DA and original model are greatest at annual scale, the timing of drought events was found to be most affected. In basins with a long-term trend (such as the Euphrates and Brahmaputra River Basins), bigger errors might be expected when using purely modeled data, especially in detecting the onset, termination and duration of droughts. In such cases, the magnitude of droughts remained less affected but in some cases the sign of SSIs was reversed, as in Yukon. From our results, the most challenging basins, where the usage of pure hydrological models might mislead the interpretations, were those exhibiting multi-year trends and seasonal (amplitude) differences. For example, in the Danube River Basin, the duration and magnitude of the severe 2019–2021 drought was not correctly reflected in the SSIs if the model was not improved by GRACE/GRACE-FO integration.

Funding

This research was funded by the Danmarks Frie Forskningsfond [10.46540/2035-00247B] for the DFF2 DANSk-LSM project. Nooshin Mehrnegar was funded by the Marie Skłodowska-Curie Actions (MSCA) postdoctoral Fellowship [101068561] for the MuSe-BDA project. The following projects partially supported CK Shum: National Geospatial-Intelligence Agency (NGA) GEO-ESCON Program (HM157522D0009, Task 8.8), and United States Agency for International Development (USAID)/Indian Partnerships Program (CA 72038621CA00002).

CRediT authorship contribution statement

Ehsan Forootan: Conceptualization, Funding acquisition, Methodology, Project administration, Resources, Writing – original draft, Writing – review & editing, Supervision, Formal analysis, Investigation, Software. **Nooshin Mehrnegar:** Data curation, Formal analysis, Methodology, Software, Validation, Visualization, Writing – original draft. **Maike Schumacher:** Conceptualization, Methodology, Supervision, Validation, Writing – review & editing. **Leire Anne Retegui Schiettekatte:** Data curation, Investigation, Writing – review & editing. **Thomas Jagdhuber:** Data curation, Validation, Writing – review & editing. **Saeed Farzaneh:** Formal analysis, Validation, Writing – review & editing. **Albert I.J.M. van Dijk:** Data curation, Investigation, Writing – review & editing. **Mohammad Shamsudduha:** Validation, Writing – review & editing. **C.K. Shum:** Data curation, Validation, Writing – review & editing.

Declaration of competing interest

The authors declare that they have no known competing financial interests or personal relationships that could have appeared to influence the work reported in this paper.

Data availability

The authors confirm that the data supporting the findings of this study are publicly available.•

Reconstructed GRACE/GRACE-FO data can be downloaded from: https://github.com/AAUGeodesy/Reconstructed-GRACE-GRACE-FO-TWSC.git,•

Global gridded groundwater SSIs from: https://github.com/AAUGeodesy/Standardize-Storage-Indeces.git, and•

Global MCMC-DA water storage changes from:• https://github.com/AAUGeodesy/MCMC-DA-water-storage-changes.git.

Acknowledgment

Authors are grateful to the comments of editors and the two anonymous reviewers, which helped to improve the quality of this article. We are also very grateful to the data products and the model codes that were freely available to conduct this research.

Appendix A. Evaluation of groundwater storage changes using in-situ groundwater measurement within Bangladesh

To evaluate the performance of MCMC-DA, besides the USGS groundwater level observation within the USA that was already performed in (Mehrnegar et al., 2020b), we used the groundwater level time series from 265 monitoring stations from the national network operated by the Bangladesh Water Development Board (BWDB). Time series data were processed by (Shamsudduha et al., 2022) and aggregated within 13 grids ($1^\circ \times 1^\circ$) to cover the entire Bangladesh. Fig. A.1 shows a comparison between the W3RA groundwater storage changes and those of derived from MCMC-DA, in terms of temporal correlation coefficients with the level measurements for the available period of 2003–2018.

The obtained results indicate that while both W3RA and MCMC-DA groundwater storage are highly correlated with in-situ data (correlations bigger than 0.7), MCMC-DA slightly improved the correlations with in-situ measurements. However, to understand the impact on the actual water storage estimates, a comparison is done between after converting the groundwater level measurements to storage estimated. For this, a specific yield of 0.01 is used (Shamsudduha et al., 2011) for the conversion, and the results of 5 stations are shown in Fig. A.1. We selected those stations that had similar correlation coefficients with the water level measurements, when using the original W3RA and MCMC-DA outputs. The results indicate that, after implementing MCMC-DA, the magnitude of model-derived groundwater storage changes is considerably changed to be close to those of in-situ observations, where the Root Mean Square of Differences (RMSD) are reduced from around 180 mm to 97 mm in Fig. A.1(a), or from 155 mm to 88 mm in Fig. A.1(b). It is worth mentioning here that in this study we only investigate whether the magnitude of the DA results is closer to the measurements (than the original model), and the absolute magnitude of the in-situ water storage is not our focus. A realistic conversion of the in-situ groundwater level to groundwater storage needs more investigations (than simply using a constant converter as applied here).

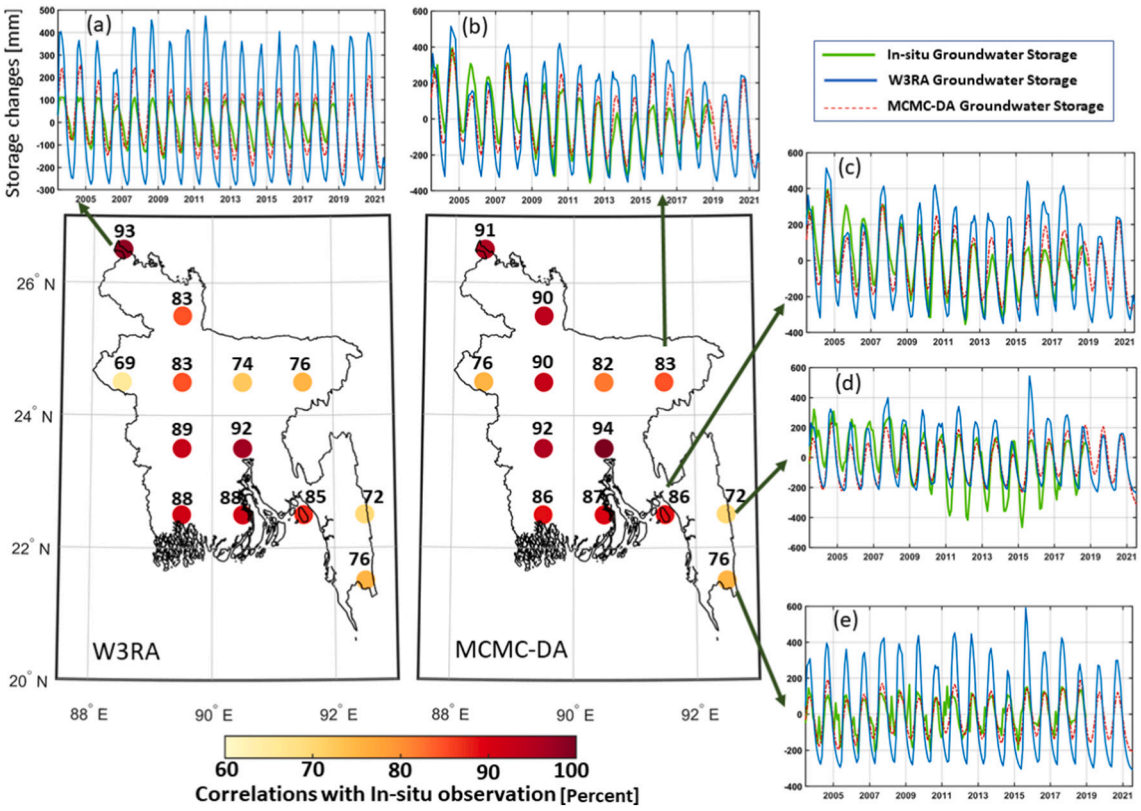

Fig. A.1. Temporal correlation coefficients (in percentage) between in-situ groundwater level changes and the storage changes of the original W3RA and MCMC-DA within Bangladesh, covering 2003–2018. A comparison between the time series of groundwater storage changes are shown for five selected stations.

Appendix B. An overview of the world's 33 large-scale river basins

The world's 33 large river basins that are considered in this study to evaluate groundwater storage changes and drought indices before and after MCMC-DA assimilation are shown in Fig. B.1. These river basins contours are based on masks of 0.5° resolution from (Oki and Sud, 1998) where among them, we show Amazon, Amur, Euphrates, Aral, Caspian, Ob, Yukon, Zambezi, Brahmaputra, Danube, and Mekong to compute the basin averages from groundwater storage changes of the model, before and after implementing MCMC-DA, and their associated SSIs.

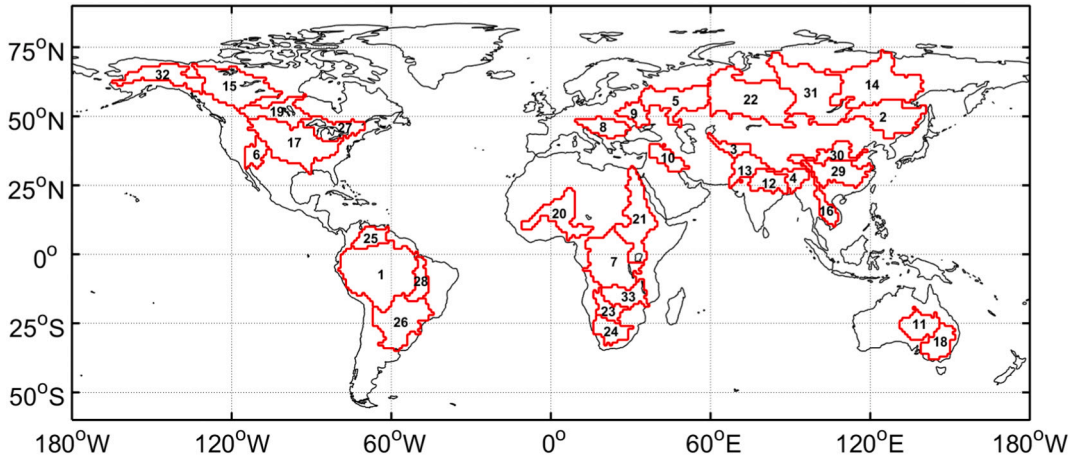

Fig. B.1. The world's 33 largest river basins are examined in this study. Each river basin is presented with a numerical label including: 1:Amazon, 2:Amur, 3:Aral, 4: Brahmaputra, 5:Caspian-Volga, 6:Colorado, 7:Congo, 8:Danube, 9:Dnieper, 10:Euphrates, 11:Lake Eyre, 12:Ganges, 13:Indus, 14:Lena, 15:Mackenzie, 16:Mekong, 17:Mississippi, 18:Murray, 19:Nelson, 20:Niger, 21:Nile, 22:Ob, 23:Okavango, 24:Orange, 25:Orinoco, 26:Parana, 27:St. Lawrence, 28:Tocantins, 29:Yangtze, 30: Yellow, 31:Yenisei, 32:Yukon, and 33:Zambezi.

Appendix C. Basin averaged comparison of the MCMC-DA and W3RA water storage changes

Changes in the water storage components of W3RA before and after integrating with the GRACE and GRACE-FO observations (through MCMC-DA) are found to be considerable. Fig. C.2 presents the results for the Euphrates River Basin. Considering the magnitude of the updates, we see that our integration introduces a big portion of updates to the deep soil and groundwater compartments. The surface water storage and snow compartments are

not considerably changed. The amplitude of the annual variability of the top soil and shallow soil compartments has been changed respectively by ~40 % and 100 %, e.g., during 2003–2009. However, the dynamics of the updates, introduced to the top layers, might be interpreted with cautions. We recommend to apply a constraint against soil moisture remote sensing products, as e.g., in (Mehrnegar et al., 2023), to achieve a more reliable drought monitoring of the close to surface compartments.

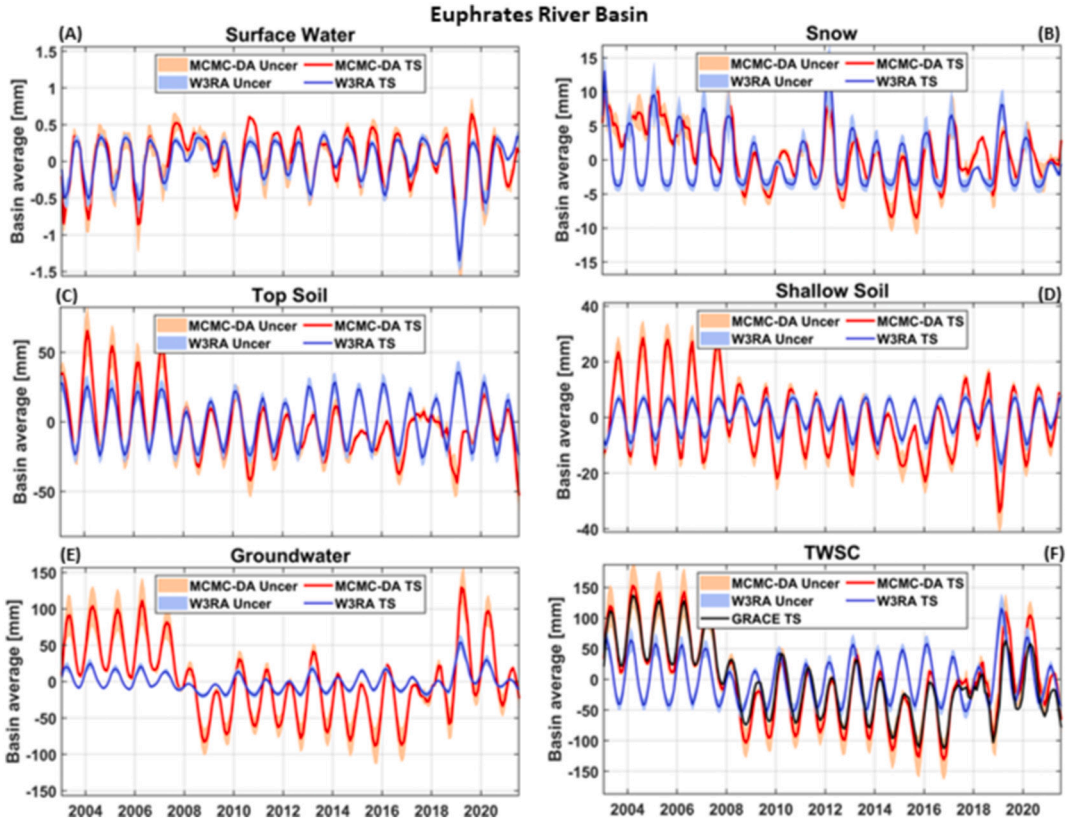

Fig. C.2. Basin averaged time series of MCMC-DA and W3RA water storage compartments within the Euphrates River Basin.

Appendix D. Reducing phase shifts in water storage changes by MCMC-DA

In this appendix, we present the timing impact of integrating GRACE and GRACE-FO TWS into a large-scale hydrological model. Fig. D.1 shows differences of the annual phase between GRACE/GRACE-FO TWS changes and those derived from the original W3RA model outputs (left), and the MCMC-DA (right) outputs. These results indicate that MCMC-DA performed well in reducing the phase differences between the modeled and measured TWS changes, where the median of phase differences between the annual amplitude of W3RA and GRACE TWSC is considerably reduced from ±180 deg. to zero after implementing MCMC-DA. These results can be interpreted as modification in the seasonal evolution of the TWS changes, where a phase modification of up to 6 months can be detected globally.

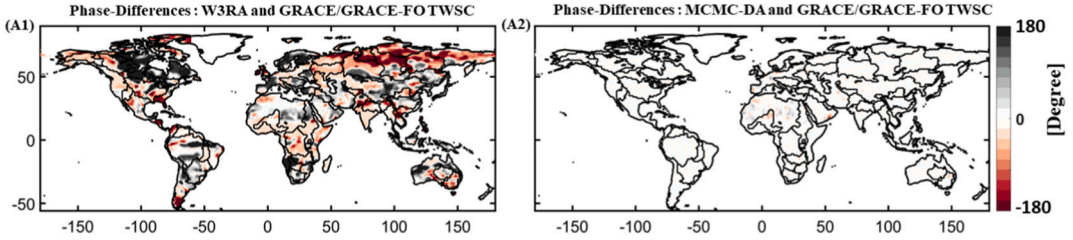

Fig. D.1. Phase differences between the GRACE and GRACE-FO TWS changes and those of the original (left) and MCMC-DA (right), i.e., after the Bayesian integration with the GRACE and GRACE-FO TWS changes.

References

Abdelmohsen, K., Sultan, M., Save, H., Abotalib, A.Z., Yan, E., Zahran, K.H., 2022. Buffering the impacts of extreme climate variability in the highly engineered Tigris Euphrates River system. Sci. Rep. 12 (1), 4178. https://doi.org/10.1038/s41598-022-07891-0.

Ahmadalipour, A., Moradkhani, H., Yan, H., Zarekarizi, M., 2017. Remote sensing of drought: vegetation, soil moisture, and data assimilation. In: Remote Sensing of Hydrological Extremes. Springer, pp. 121–149. https://doi.org/10.1007/978-3-319-43744-6_7.

Anyah, R., Forootan, E., Awange, J.L., Khaki, M., 2018. Understanding linkages between global climate indices and terrestrial water storage changes over Africa using GRACE products. Sci. Total Environ. 635, 1405–1416. https://doi.org/10.1016/j.scitotenv.2018.04.159.

Argus, D.F., Peltier, W., Drummond, R., Moore, A.W., 2014. The Antarctica component of postglacial rebound model ice-6g_c (vm5a) based on gps positioning, exposure age

dating of ice thicknesses, and relative sea level histories. Geophys. J. Int. 198 (1), 537–563. https://doi.org/10.1093/GJI/GGU140.
Awange, J.L., Ferreira, V., Forootan, E., Khandu, S., Andam-Akorful, N., Agutu, X. He, 2016. Uncertainties in remotely sensed precipitation data over Africa. Int. J. Climatol. 36 (1), 303–323. https://doi.org/10.1002/joc.4346.
Baguis, P., Carrassi, A., Roulin, E., Vannitsem, S., Modanesi, S., Lievens, H., Bechtold, M., De Lannoy, G., 2022. Assimilation of backscatter observations into a hydrological model: a case study in Belgium using ASCAT data. Remote Sens. 14, 5740. https://doi.org/10.3390/rs14225740.
Barbosa, P. Marinho Ferreira, Masante, D., Arias-Munoz, C., Cammalleri, C., De Jager, A., Magni, D., Mazzeschi, M., Mccormick, N., Naumann, G., Spinoni, J., Vogt, J., 2021. Droughts in Europe and worldwide 2019–2020 (KJ-NA-30719-EN-N). https://doi.org/10.2760/415204.
Bernstein, D.S., 2005. Matrix Mathematics: Theory, Facts, and Formulas With Application to Linear Systems Theory, Vol. 41. Princeton University Press, Princeton.
Bezděk, A., Sebera, J., Teixeira da Encarnação, J., Klokočník, J., 2016. Time-variable gravity fields derived from GPS tracking of Swarm. Geophys. J. Int. 205 (3), 1665–1669. https://doi.org/10.1093/gji/ggw094.
Bolaños Chavarría, S., Werner, M., Salazar, J.F., Betancur Vargas, T., 2022. Benchmarking global hydrological and land surface models against GRACE in a medium-sized tropical basin. Hydrol. Earth Syst. Sci. 26 (16), 4323–4344. https://doi.org/10.5194/hess-26-4323-2022.
Boljka, L., Omrani, N.-E., Keenlyside, N.S., 2022. Identifying quasi-periodic variability using multivariate empirical mode decomposition: a case of the tropical pacific. Weather and Climate Dynamics Discussions 2022, 1–40. https://doi.org/10.5194/wcd-2022-51 (URL https://wcd.copernicus.org/preprints/wcd-2022-51/).
Carrão, H., Russo, S., Sepulcre-Canto, G., Barbosa, P., 2016. An empirical standardized soil moisture index for agricultural drought assessment from remotely sensed data. Int. J. Appl. Earth Obs. Geoinf. 48, 74–84. https://doi.org/10.1016/j.jag.2015.06.011.
Chen, J.L., Wilson, C.R., Famiglietti, J.S., Rodell, M., 2007. Attenuation effect on seasonal basin-scale water storage changes from GRACE time-variable gravity. J. Geodyn. 81 (4), 237–245. https://doi.org/10.1007/s00190-006-0104-2.
Dai, A., 2013. Increasing drought under global warming in observations and models. Nat. Clim. Chang. 3 (1), 52–58. https://doi.org/10.1038/nclimate1633.
Davey, M., Brookshaw, A., Ineson, S., 2014. The probability of the impact of ENSO on precipitation and near-surface temperature, climate. Risk Manage. 1, 5–24. https://doi.org/10.1016/j.crm.2013.12.002.
Dutra, E., Wetterhall, F., Giuseppe, F.D., Naumann, G., Barbosa, P., Vogt, J., Pozzi, W., Pappenberger, F., 2014. Global meteorological drought–part 1: probabilistic monitoring. Hydrol. Earth Syst. Sci. 18 (7), 2657–2667. https://doi.org/10.5194/hess-18-2657-2014.
Dutta, R., 2015. Remote sensing of energy fluxes and soil moisture content. https://doi.org/10.1080/14498596.2015.1006114.
Edwards, D.C., 1997. Characteristics of 20th Century Drought in the United States at Multiple Time Scales. Tech. rep, AIR FORCE INST OF TECH WRIGHT-PATTERSON AFB OH.
Eicker, A., Forootan, E., Springer, A., Longuevergne, L., Kusche, J., 2016. Does GRACE see the terrestrial water cycle "intensifying"? J. Geophys. Res. Atmos. 121 (2), 733–745. https://doi.org/10.1002/2015JD023808.
Famiglietti, J., Cazenave, A., Eicker, A., Reager, J., Rodell, M., Velicogna, I., 2015. Satellites provide the big picture. Science (New York, N.Y.) 349 (6249), 684–685. https://doi.org/10.1126/science.aac9238.
Ferreira, V., Yong, B., Montecino, H., Ndehedehe, C.E., Seitz, K., Kutterer, H., Yang, K., 2023. Estimating grace terrestrial water storage anomaly using an improved point mass solution. Sci. Data 10 (1), 234. https://doi.org/10.1038/s41597-023-02122-1.
Ferreira, V.G., Montecino, H.D.C., Yakubu, C.I., Heck, B., 2016. Uncertainties of the Gravity Recovery and Climate Experiment time-variable gravity-field solutions based on three-cornered hat method. J. Appl. Remote. Sens. 10 (1), 1–20. https://doi.org/10.1117/1.JRS.10.015015.
Forootan, E., Kusche, J., 2013. Separation of deterministic signals using Independent Component Analysis (ICA). Stud. Geophys. Geod. 57 (1), 17–26. https://doi.org/10.1007/s11200-012-0718-1.
Forootan, E., Mehrnegar, N., 2022. A hierarchical constrained bayesian (conbay) approach to jointly estimate water storage and post-glacial rebound from GRACE (-FO) and GNSS data. All Earth 34 (1), 120–146. https://doi.org/10.1080/27669645.2022.2097768.
Forootan, E., Awange, J.L., Kusche, J., Heck, B., Eicker, A., 2012. Independent patterns of water mass anomalies over Australia from satellite data and models. Remote Sens. Environ. 124, 427–443. https://doi.org/10.1016/j.rse.2012.05.023.
Forootan, E., Didova, O., Schumacher, M., Kusche, J., Elsaka, B., 2014. Comparisons of atmospheric mass variations derived from ECMWF reanalysis and operational fields, over 2003–2011. J. Geod. 88 (5), 503–514. https://doi.org/10.1007/s00190-014-0696-x.
Forootan, E., Awange, J., Schumacher, M., Anyah, R., van Dijk, A.I.J.M., Kusche, J., et al., 2016. Quantifying the impacts of enso and iod on rain gauge and remotely sensed precipitation products over Australia. Remote Sens. Environ. 172, 50–66. https://doi.org/10.1016/j.rse.2015.10.027.
Forootan, E., Safari, A., Mostafaie, A., Schumacher, M., Delavar, M., Awange, J.L., 2017. Large-scale total water storage and water flux changes over the arid and semiarid parts of the Middle East from GRACE and reanalysis products. Surv. Geophys. 38 (3), 591–615. https://doi.org/10.1007/s10712-016-9403-1.
Forootan, E., Kusche, J., Talpe, M., Shum, C.K., Schmidt, M., 2018. Developing a Complex Independent Component Analysis (CICA) technique to extract non-stationary patterns from geophysical time series. Surv. Geophys. 39, 35–465. https://doi.org/10.1007/s10712-017-9451-1.
Forootan, E., Khaki, M., Schumacher, M., Wulfmeyer, V., Mehrnegar, N., van Dijk, A.I.J.M., Brocca, L., Farzaneh, S., Akinluyi, F., Ramillien, G., et al., 2019. Understanding the global hydrological droughts of 2003–2016 and their relationships with teleconnections. Sci. Total Environ. 650, 2587–2604. https://doi.org/10.1016/j.scitotenv.2018.09.231.
Forootan, E., Schumacher, M., Mehrnegar, N., Bezděk, A., Talpe, M.J., Farzaneh, S., Zhang, C., Zhang, Y., Shum, C.K., 2020. An iterative ICA-based reconstruction method to produce consistent time-variable total water storage fields using GRACE and Swarm satellite data. Remote Sens. 12 (10), 1639. https://doi.org/10.3390/rs12101639.
Frappart, F., Ramillien, G., 2018. Monitoring groundwater storage changes using the Gravity Recovery and Climate Experiment (GRACE) satellite mission: a review. Remote Sens. 10 (6), 829. https://doi.org/10.3390/rs10060829.
Gelfand, A.E., Smith, A.F.M., 1990. Sampling-based approaches to calculating marginal densities. J. Am. Stat. Assoc. 85 (410), 398–409. https://doi.org/10.1080/01621459.1990.10476213.
Girotto, M., De Lannoy, G.J., Reichle, R.H., Rodell, M., 2016. Assimilation of gridded terrestrial water storage observations from GRACE into a land surface model. Water Resour. Res. 52 (5), 4164–4183. https://doi.org/10.1002/2015WR018417.
Girotto, M., De Lannoy, G.J., Reichle, R.H., Rodell, M., Draper, C., Bhanja, S.N., Mukherjee, A., 2017. Benefits and pitfalls of GRACE data assimilation: a case study of terrestrial water storage depletion in India. Geophys. Res. Lett. 44 (9), 4107–4115. https://doi.org/10.1002/2017GL072994.
Guttman, N.B., 1999. Accepting the standardized precipitation index: a calculation algorithm 1. J. Am. Water Resour. Assoc. 35 (2), 311–322. https://doi.org/10.1111/j.1752-1688.1999.tb03592.x.
Hao, Z., AghaKouchak, A., 2013. Multivariate standardized drought index: a parametric multi-index model. Adv. Water Resour. 57, 12–18. https://doi.org/10.1016/j.advwatres.2013.03.009.
Hao, Z., Yuan, X., Xia, Y., Hao, F., Singh, V.P., 2017. An overview of drought monitoring and prediction systems at regional and global scales. Bull. Am. Meteorol. Soc. 98 (9), 1879–1896. https://doi.org/10.1175/BAMS-D-15-00149.1.
Hersbach, H., Dee, D., 2016. ERA5 reanalysis is in production. ECMWF Newsletter 147 (7), 5–6. https://doi.org/10.24381/cds.adbb2d47.
Houborg, R., Rodell, M., Li, B., Reichle, R., Zaitchik, B.F., 2012. Drought indicators based on model-assimilated Gravity Recovery and Climate Experiment (GRACE) terrestrial water storage observations. Water Resour. Res. 48 (7) https://doi.org/10.1029/2011WR011291.
Jolliffe, I.T., 1986. Principal Components in Regression Analysis. Springer, New York, New York, NY, pp. 129–155. https://doi.org/10.1007/978-1-4757-1904-8_8.
Khaki, M., Forootan, E., Kuhn, M., Awange, J.L., Papa, F., Shum, C.K., 2018. A study of Bangladesh's sub-surface water storages using satellite products and data assimilation scheme. Sci. Total Environ. 625, 963–977. https://doi.org/10.1016/j.scitotenv.2017.12.289.
Kitagawa, G., 1987. Non-Gaussian state—space modeling of nonstationary time series. J. Am. Stat. Assoc. 82 (400), 1032–1041. https://doi.org/10.1080/01621459.1987.10478534.
Koch, K.-R., 2007. Introduction to Bayesian Statistics. Springer Science & Business Media.
Kumar, S., Kolassa, J., Reichle, R., Crow, W., de Lannoy, G., de Rosnay, P., MacBean, N., Girotto, M., Fox, A., Quaife, T., et al., 2022. An agenda for land data assimilation priorities: realizing the promise of terrestrial water, energy, and vegetation observations from space. J. Adv. Model. Earth Syst. 14 (11), e2022MS003259 https://doi.org/10.1029/2022MS003259.
Kusche, J., Schmidt, R., Petrovic, S., Rietbroek, R., 2009. Decorrelated GRACE time-variable gravity solutions by GFZ, and their validation using a hydrological model. J. Geodyn. 83 (10), 903–913. https://doi.org/10.1007/s00190-009-0308-3.
Landerer, F.W., Flechtner, F.M., Save, H., Webb, F.H., Bandikova, T., Bertiger, W.I., Bettadpur, S.V., Byun, S.H., Dahle, C., Dobslaw, H., et al., 2020. Extending the global mass change data record: GRACE Follow-On instrument and science data performance. Geophys. Res. Lett. 47 (12), e2020GL088306 https://doi.org/10.1029/2020GL088306.
Lievens, H., Tomer, S.K., Al Bitar, A., De Lannoy, G.J., Drusch, M., Dumedah, G., Franssen, H.-J.H., Kerr, Y.H., Martens, B., Pan, M., et al., 2015. SMOS soil moisture assimilation for improved hydrologic simulation in the Murray Darling Basin, Australia. Remote Sens. Environ. 168, 146–162. https://doi.org/10.1016/j.rse.2015.06.025.
Liu, Y., Gupta, H.V., 2007. Uncertainty in hydrologic modeling: toward an integrated data assimilation framework. Water Resour. Res. 43 (7) https://doi.org/10.1029/2006WR005756.
Llovel, W., Becker, M., Cazenave, A., Jevrejeva, S., Alkama, R., Decharme, B., Douville, H., Ablain, M., Beckley, B., 2011. Terrestrial waters and sea level variations on interannual time scale. Glob. Planet. Chang. 75 (1–2), 76–82. https://doi.org/10.1016/j.gloplacha.2010.10.008.
McKee, T.B., Doesken, N.J., Kleist, J., et al., 1993. The relationship of drought frequency and duration to time scales. In: Proceedings of the 8th Conference on Applied Climatology, Vol. 17, pp. 179–183 (Boston).
Mehrnegar, N., Jones, O., Singer, M.B., Schumacher, M., Bates, P., Forootan, E., 2020a. Comparing global hydrological models and combining them with GRACE by Dynamic Model Data Averaging (DMDA). Adv. Water Resour. 138, 103528 https://doi.org/10.1016/j.advwatres.2020.103528.
Mehrnegar, N., Jones, O., Singer, M.B., Schumacher, M., Jagdhuber, T., Scanlon, B.R., Rateb, A., Forootan, E., 2020b. Exploring groundwater and soil water storage changes across the CONUS at 12.5 km resolution by a Bayesian integration of GRACE data into W3RA. Sci. Total Environ. 758, 143579 https://doi.org/10.1016/j.scitotenv.2020.143579.

Mehrnegar, N., Schumacher, M., Jagdhuber, T., Forootan, E., 2023. Making the best use of GRACE, GRACE-FO and SMAP data through a constrained Bayesian data-model integration. Water Resour. Res. 59, e2023WR034544 https://doi.org/10.1029/2023WR034544.

Melkonian, A.K., Willis, M.J., Pritchard, M.E., 2014. Satellite-derived volume loss rates and glacier speeds for the Juneau icefield, Alaska. J. Glaciol. 60 (222), 743–760. https://doi.org/10.3189/2014JoG13J181.

Mishra, A., Vu, T., Veettil, A.V., Entekhabi, D., 2017. Drought monitoring with Soil Moisture Active Passive (SMAP) measurements. J. Hydrol. 552, 620–632. https://doi.org/10.1016/j.jhydrol.2017.07.033 (URL https://www.sciencedirect.com/science/article/pii/S0022169417304821).

Mishra, A.K., Singh, V.P., 2010. A review of drought concepts. J. Hydrol. 391 (1–2), 202–216. https://doi.org/10.1016/j.jhydrol.2010.07.012.

Muñoz Sabater, J., et al., 2019. Era5-land hourly data from 1981 to present, Copernicus Climate Change Service (C3S). Climate Data Store (CDS) 10. https://doi.org/10.24381/cds.e2161bac.

Oki, T., Sud, Y., 1998. Design of total runoff integrating pathways (trip)—a global river channel network. Earth Interact. 2 (1), 1–37. https://doi.org/10.1175/1087-3562(1998)002<0001:DOTRIP>2.3.CO;2.

Pan, M., Wood, E.F., 2006. Data assimilation for estimating the terrestrial water budget using a constrained ensemble Kalman filter. J. Hydrometeorol. 7 (3), 534–547. https://doi.org/10.1175/JHM495.1.

Pan, M., Sahoo, A.K., Troy, T.J., Vinukollu, R.K., Sheffield, J., Wood, E.F., 2012. Multisource estimation of long-term terrestrial water budget for major global river basins. J. Clim. 25 (9), 3191–3206. https://doi.org/10.1175/JCLI-D-11-00300.1.

Pandey, A., Prakash, A., Barua, A., Abu Syed, M., Nepal, S., 2020. Upstream-downstream linkages in Ganges-Brahmaputra-Meghna Basin: the hydro-social imperatives. Water Policy 22 (6), 1082–1097. https://doi.org/10.2166/wp.2020.231.

Parajuli, B., Zhang, X., Deuja, S., Liu, Y., 2021. Regional and seasonal precipitation and drought trends in Ganga–Brahmaputra Basin. Water 13 (16), 2218. https://doi.org/10.3390/w13162218.

Peltier, W.R., Argus, D., Drummond, R., 2015. Space geodesy constrains ice age terminal deglaciation: the global ice-6g_c (vm5a) model. J. Geophys. Res. Solid Earth 120 (1), 450–487. https://doi.org/10.1002/2014JB011176.

Phillips, T., Nerem, R.S., Fox-Kemper, B., Famiglietti, J.S., Rajagopalan, B., 2012. The influence of ENSO on global terrestrial water storage using GRACE. Geophys. Res. Lett. 39 (16) https://doi.org/10.1029/2012GL052495.

Pozzi, W., Sheffield, J., Stefanski, R., Cripe, D., Pulwarty, R., Vogt, J.V., Heim, R.R., Brewer, M.J., Svoboda, M., Westerhoff, R., et al., 2013. Toward global drought early warning capability: expanding international cooperation for the development of a framework for monitoring and forecasting. Bull. Am. Meteorol. Soc. 94 (6), 776–785. https://doi.org/10.1175/BAMS-D-11-00176.1.

Reichle, R.H., Koster, R.D., 2005. Global assimilation of satellite surface soil moisture retrievals into the nasa catchment land surface model. Geophys. Res. Lett. 32 (2) https://doi.org/10.1029/2004GL021700.

Renzullo, L.J., van Dijk, A.I.J.M., Perraud, J.-M., Collins, D., Henderson, B., Jin, H., Smith, A., McJannet, D.L., 2014. Continental satellite soil moisture data assimilation improves root-zone moisture analysis for water resources assessment. J. Hydrol. 519, 2747–2762. https://doi.org/10.1016/j.jhydrol.2014.08.008.

Richard Peltier, W., Argus, D.F., Drummond, R., 2018. Comment on "an assessment of the ice-6g_c (vm5a) glacial isostatic adjustment model" by Purcell et al. J. Geophys. Res. Solid Earth 123 (2), 2019–2028. https://doi.org/10.1002/2016JB013844.

Scanlon, B.R., Zhang, Z., Save, H., Sun, A.Y., Schmied, H.M., van Beek, L.P., Wiese, D.N., Wada, Y., Long, D., Reedy, R.C., et al., 2018. Global models underestimate large decadal declining and rising water storage trends relative to GRACE satellite data. Proc. Natl. Acad. Sci. 115 (6), E1080–E1089. https://doi.org/10.1073/pnas.1704665115.

Scanlon, B.R., Rateb, A., Anyamba, A., Kebede, S., MacDonald, A.M., Shamsudduha, M., Small, J., Sun, A., Taylor, R.G., Xie, H., 2022. Linkages between GRACE water storage, hydrologic extremes, and climate teleconnections in major African aquifers. Environ. Res. Lett. 17 (1), 014046 https://doi.org/10.1088/1748-9326/ac3bfc.

Schumacher, M., 2016. Methods for Assimilating Remotely-sensed Water Storage Changes Into Hydrological Models. Ph.D. thesis,. Universitäts-und Landesbibliothek Bonn.

Schumacher, M., Forootan, E., van Dijk, A.I.J.M., Schmied, H.M., Crosbie, R.S., Kusche, J., Döll, P., 2018. Improving drought simulations within the Murray-Darling Basin by combined calibration/assimilation of GRACE data into the WaterGAP Global Hydrology Model. Remote Sens. Environ. 204, 212–228. https://doi.org/10.1016/j.rse.2017.10.029.

Shamsudduha, M., Taylor, R.G., Ahmed, K.M., Zahid, A., 2011. The impact of intensive groundwater abstraction on recharge to a shallow regional aquifer system: evidence from Bangladesh. Hydrogeol. J. 19 (4), 901. https://doi.org/10.1007/s10040-011-0723-4.

Shamsudduha, M., Taylor, R.G., Haq, M.I., Nowreen, S., Zahid, A., Ahmed, K.M.U., 2022. The Bengal water machine: quantified freshwater capture in Bangladesh. Science 377 (6612), 1315–1319. https://doi.org/10.1126/science.abm4730.

Sheffield, J., Wood, E.F., 2012. Drought: Past Problems and Future Scenarios. Routledge.

Sinha, D., Syed, T.H., Famiglietti, J.S., Reager, J.T., Thomas, R.C., 2017. Characterizing drought in India using GRACE observations of terrestrial water storage deficit. J. Hydrometeorol. 18 (2), 381–396. https://doi.org/10.1175/JHM-D-16-0047.1.

Smith, A.B., Katz, R.W., 2013. US billion-dollar weather and climate disasters: data sources, trends, accuracy and biases. Nat. Hazards 67 (2), 387–410. https://doi.org/10.1007/s11069-013-0566-5.

Smith, A.F.M., Roberts, G.O., 1993. Bayesian computation via the Gibbs sampler and related Markov chain Monte Carlo methods. J. R. Stat. Soc. B. Methodol. 55 (1), 3–23. https://doi.org/10.1111/j.2517-6161.1993.tb01466.x.

Swenson, S., Chambers, D., Wahr, J., 2008. Estimating geocenter variations from a combination of GRACE and ocean model output. J. Geophys. Res. Solid Earth 113 (B8). https://doi.org/10.1029/2007JB005338.

Tangdamrongsub, N., Han, S.-C., Yeo, I.-Y., Dong, J., Steele-Dunne, S.C., Willgoose, G., Walker, J.P., 2020. Multivariate data assimilation of GRACE, SMOS, SMAP measurements for improved regional soil moisture and groundwater storage estimates. Adv. Water Resour. 135, 103477 https://doi.org/10.1016/j.advwatres.2019.103477.

Tapley, B.D., Bettadpur, S., Watkins, M., Reigber, C., 2004. The gravity recovery and climate experiment: mission overview and early results. Geophys. Res. Lett. 31 (9) https://doi.org/10.1029/2004GL019779.

Tapley, B.D., Watkins, M.M., Flechtner, F., Reigber, C., Bettadpur, S., Rodell, M., Sasgen, I., Famiglietti, J.S., Landerer, F.W., Chambers, D.P., et al., 2019. Contributions of GRACE to understanding climate change. Nat. Clim. Chang. 9 (5), 358–369. https://doi.org/10.1038/s41558-019-0456-2.

Toreti, A., Bavera, D., Acosta, N.J., Cammalleri, C., De, J.A., Di, C.C., Hrast, E.A., Maetens, W., Magni, D., Masante, D., Mazzeschi, M., Niemeyer, S., Spinoni, J., 2022. Drought in Europe August 2022. Publications Office of the European Union JRC130493. https://doi.org/10.2760/264241.

Trenberth, K.E., Hoar, T.J., 1996. The 1990–1995 El Niño-Southern Oscillation event: longest on record. Geophys. Res. Lett. 23 (1), 57–60. https://doi.org/10.1029/95GL03602.

Uebbing, B., Forootan, E., Braakmann-Folgmann, A., Kusche, J., 2017. Inverting surface soil moisture information from satellite altimetry over arid and semi-arid regions. Remote Sens. Environ. 196, 205–223. https://doi.org/10.1016/j.rse.2017.05.004.

van Dijk, A.I.J.M., 2010. The Australian Water Resources Assessment System: Technical 901 Report 3, Landscape Model (Version 0.5) Technical Description, CSIRO, Water for a Healthy Country National Research Flagship.

van Dijk, A.I.J.M., Renzullo, L.J., Wada, Y., Tregoning, P., 2014. A global water cycle reanalysis (2003−2012) merging satellite gravimetry and altimetry observations with a hydrological multi-model ensemble. Hydrol. Earth Syst. Sci. 18 (8), 2955–2973. https://doi.org/10.5194/hess-18-2955-2014.

van Dijk, A.I.J.M., Schellekens, J., Yebra, M., Beck, H.E., Renzullo, L.J., Weerts, A., Donchyts, G., 2018. Global 5 km resolution estimates of secondary evaporation including irrigation through satellite data assimilation. Hydrol. Earth Syst. Sci. 22 (9), 4959–4980. https://doi.org/10.5194/hess-22-4959-2018 (URL https://hess.copernicus.org/articles/22/4959/2018/).

Van Loon, A., Laaha, G., 2015. Hydrological drought severity explained by climate and catchment characteristics. J. Hydrol. 526, 3–14. https://doi.org/10.1016/j.jhydrol.2014.10.059.

Van Loon, A.F., 2015. Hydrological drought explained. Wiley Interdiscip. Rev. Water 2 (4), 359–392. https://doi.org/10.1002/wat2.1085.

Vicente-Serrano, S.M., Beguería, S., López-Moreno, J.I., 2010. A multiscalar drought index sensitive to global warming: the standardized precipitation evapotranspiration index. J. Clim. 23 (7), 1696–1718. https://doi.org/10.1175/2009JCLI2909.1.

Vishwakarma, B.D., Horwath, M., Devaraju, B., Groh, A., Sneeuw, N., 2017. A data-driven approach for repairing the hydrological catchment signal damage due to filtering of GRACE products. Water Resour. Res. 53 (11), 9824–9844. https://doi.org/10.1002/2017WR021150.

Voss, K.A., Famiglietti, J.S., Lo, M., De Linage, C., Rodell, M., Swenson, S.C., 2013. Groundwater depletion in the Middle East from GRACE with implications for transboundary water management in the Tigris-Euphrates-Western Iran region. Water Resour. Res. 49 (2), 904–914. https://doi.org/10.1002/wrcr.20078.

Wu, H., Hayes, M.J., Weiss, A., Hu, Q., 2001. An evaluation of the standardized precipitation index, the China-z index and the statistical z-score. Int. J. Climatol. 21 (6), 745–758. https://doi.org/10.1002/joc.658.

Xu, X., Li, J., Tolson, B.A., 2014. Progress in integrating remote sensing data and hydrologic modeling. Prog. Phys. Geogr. 38 (4), 464–498. https://doi.org/10.1177/0309133314536583.

Xu, X., Tolson, B.A., Li, J., Staebler, R.M., Seglenieks, F., Haghnegahdar, A., Davison, B., 2015. Assimilation of SMOS soil moisture over the Great Lakes Basin. Remote Sens. Environ. 169, 163–175. https://doi.org/10.1016/j.rse.2015.08.017.

Yang, J., Gong, P., Fu, R., Zhang, M., Chen, J., Liang, S., Xu, B., Shi, J., Dickinson, R., 2013. The role of satellite remote sensing in climate change studies. Nat. Clim. Chang. 3 (10), 875–883. https://doi.org/10.1038/nclimate1908.

Zaitchik, B.F., Rodell, M., Reichle, R.H., 2008. Assimilation of GRACE terrestrial water storage data into a land surface model: results for the Mississippi River basin. J. Hydrometeorol. 9 (3), 535–548. https://doi.org/10.1175/2007JHM951.1.

Zhang, L., Dobslaw, H., Thomas, M., 2016. Globally gridded terrestrial water storage variations from GRACE satellite gravimetry for hydrometeorological applications. Geophys. J. Int. 206 (1), 368–378. https://doi.org/10.1093/gji/ggw153.

Zhao, M., Velicogna, I., Kimball, J.S., 2017. A global gridded dataset of grace drought severity index for 2002–14: comparison with pdsi and spei and a case study of the Australia millennium drought. J. Hydrometeorol. 18 (8), 2117–2129. https://doi.org/10.1175/JHM-D-16-0182.1.